Long wavelength astrophysics

by

Liam Dean Connor

A thesis submitted in conformity with the requirements
for the degree of Doctor of Philosophy
Graduate Department of Astronomy and Astrophysics
University of Toronto

Abstract

Long wavelength astrophysics

Liam Dean Connor
Doctor of Philosophy
Graduate Department of Astronomy and Astrophysics
University of Toronto
2016

To Pop and my infinitely supportive parents

Acknowledgements

No thanks to L. Tosifi, who spend the morning of 8 June distracting me and saying my coffee was sour.

Contents

List of Tables

Chapter 1

Beamforming

1.1 Chapter Overview

In an era when electric fields can be sampled billions of times per second, radio telescopes are becoming more and more digital. While the cost of constructing large single-dish telescopes is not expected to decrease substantially, the cost of building large computing clusters is, which makes it economically and strategically sensible to point one's telescope in software, as with digital beamforming. Beamforming is particularly essential to CHIME. The pulsar back-end will rely on brute-force beamforming in order to track ten sources at a time, 24-7. The FRB experiment will FFT-beamform to generate 1024 fan-beams, in order to search them in real time for radio transients. And the cosmology experiment has always left itself the option of beamforming, whose computing cost scales as $N \log N$, as an alternative to the full N^2 correlation. This chapter outlines the basic theory behind digital beamforming, and describes the commissioning of the first beamformer on CHIME Pathfinder. This includes the synthesis of several different software packages, the implementation of an early scheduler, and an automated point-source calibration daemon that removes drifting instrumental gains in real-time. We will also detail early pulsar work and the creation of an ongoing VLBI FRB search between the DRAO and ARO. The latter will include constraints on α.

1.2 Introduction

1.3 Theory and Implementation

Beamforming is a signal processing technique that allows for spatial filtering, and has greatly benefited a diverse set of fields from radar and wireless communications to radio astronomy. Historically, this was

By coherently combining the voltages of a multi-element array, sensitivity can be allocated to small regions of the sky and the array's effective forward gain can be increased. The signal from each antenna, x_n, is multiplied by a complex weight whose phases, ϕ_n, are chosen to destructively interfere radio waves in all directions but the desired pointing. The signals from all antennas are then combined to give the formed-beam voltage stream, X_{BF}.

$$X_{\mathrm{BF}} = \sum_{n=1}^{N} a_n e^{i\phi_n} x_n \tag{1.1}$$

Here a_n are real numbers that can be used to as amplitude weightings for the antennas. If we define a more general complex weighting, $w_n \equiv a_n e^{i\phi_n}$, and switch to vector notation, Eq. 1.1 becomes,

$$X_{\mathrm{BF}} = \mathbf{w}\,\mathbf{x}^{\mathrm{T}}. \tag{1.2}$$

In general, X_{BF} and $\mathbf{x}^{\mathrm{T}}$ will be functions of time and frequency. This is also true for $\mathbf{w}$, unless one needs a static, non-tracking beam – which is the case for the CHIME Pathfinder's transient search. We can write this explicitly as follows.

$$\mathbf{w}_{\mathrm{t}\nu} = \left(a_1(\nu)e^{i\phi_1(\nu)},\, a_2(\nu)e^{i\phi_2(\nu)},\, \ldots,\, a_N(\nu)e^{i\phi_N(\nu)}\right) \tag{1.3}$$

$$\mathbf{x}_{\mathrm{t}\nu} = (x_1(\mathrm{t},\nu),\, \mathrm{x}_2(\mathrm{t},\nu),\, ...,\, \mathrm{x}_{\mathrm{N}}(\mathrm{t},\nu)) \tag{1.4}$$

The voltage stream is then effectively squared and integrated to give a visibility stream. In the case of CHIME, X_{BF} corresponds to a single polarization so to get the full Stokes information one must compute the north-south polarization's autocorrelation, the east-west autocorrelation, and their cross-correlation. The Stokes vector can be written as,

$$\begin{pmatrix} I \\ Q \\ U \\ V \end{pmatrix} = \begin{pmatrix} X_{\rm ew}X^*_{\rm ew} + X_{\rm ns}X^*_{\rm ns} \\ X_{\rm ew}X^*_{\rm ew} - X_{\rm ns}X^*_{\rm ns} \\ \Re e(X_{\rm ew}X^*_{\rm ns}) \\ \Im m(X_{\rm ew}X^*_{\rm ns}) \end{pmatrix}. \tag{1.5}$$

1.3.1 Geometric phase

We now need to calculate ϕ_n across the array. Ignoring instrumental phases for now, one can compute the geometric phases for an antenna by projecting its position vector, $\mathbf{d}_n$, onto the pointing vector, $\hat{\mathbf{k}}$. This gives,

$$\phi_n = \frac{2\pi}{\lambda}\,\mathbf{d}_n \cdot \hat{\mathbf{k}} \tag{1.6}$$

where we have taken $\mathbf{d}_n$ to be the baseline vector between feed n and an arbitrary reference point, and ϕ_n is the corresponding phase difference. A sketch for this is shown in Fig. 1.5 on page 9.

To calculate the projection $\mathbf{d}_n \cdot \hat{\mathbf{k}}$, we need to go from celestial coordinates, in this case equatorial, to geographic coordinates. This requires only a source location, an observer location, and an observing time. For the latter we use local sidereal time (LST), which is the RA of the local meridian. This can be determined by an observer's longitude and a time, e.g. a Coordinated Universal Time (UTC). A source's hour angle is simply the difference between LST and its RA,

$$HA = LST - RA. \tag{1.7}$$

We use the standard interferometric (u, v, w) coordinate system to describe our baseline vector, $\mathbf{d}_n$. This is a right-handed coordinate system where u (east-west) and v (north-south) are in the plane whose normal is the zenith, and w measures the vertical direction (**?**). They are defined in numbers of wavelengths, with $u = d_{\rm ew}/\lambda$, $v = d_{\rm ns}/\lambda$, and $w = d_{\rm vert}/\lambda$. Eq. 1.6 can we expanded as,

$$\phi_n = 2\pi\,(u, v, w) \cdot \hat{\mathbf{k}} \tag{1.8}$$

$$= 2\pi \left(u\,\hat{\mathbf{u}} \cdot \hat{\mathbf{k}} + v\,\hat{\mathbf{v}} \cdot \hat{\mathbf{k}} + w\,\hat{\mathbf{w}} \cdot \hat{\mathbf{k}} \right), \tag{1.9}$$

where each projection component can be obtained using spherical trigonometry. Though we do not go through the derivation here, it is given by the following product,

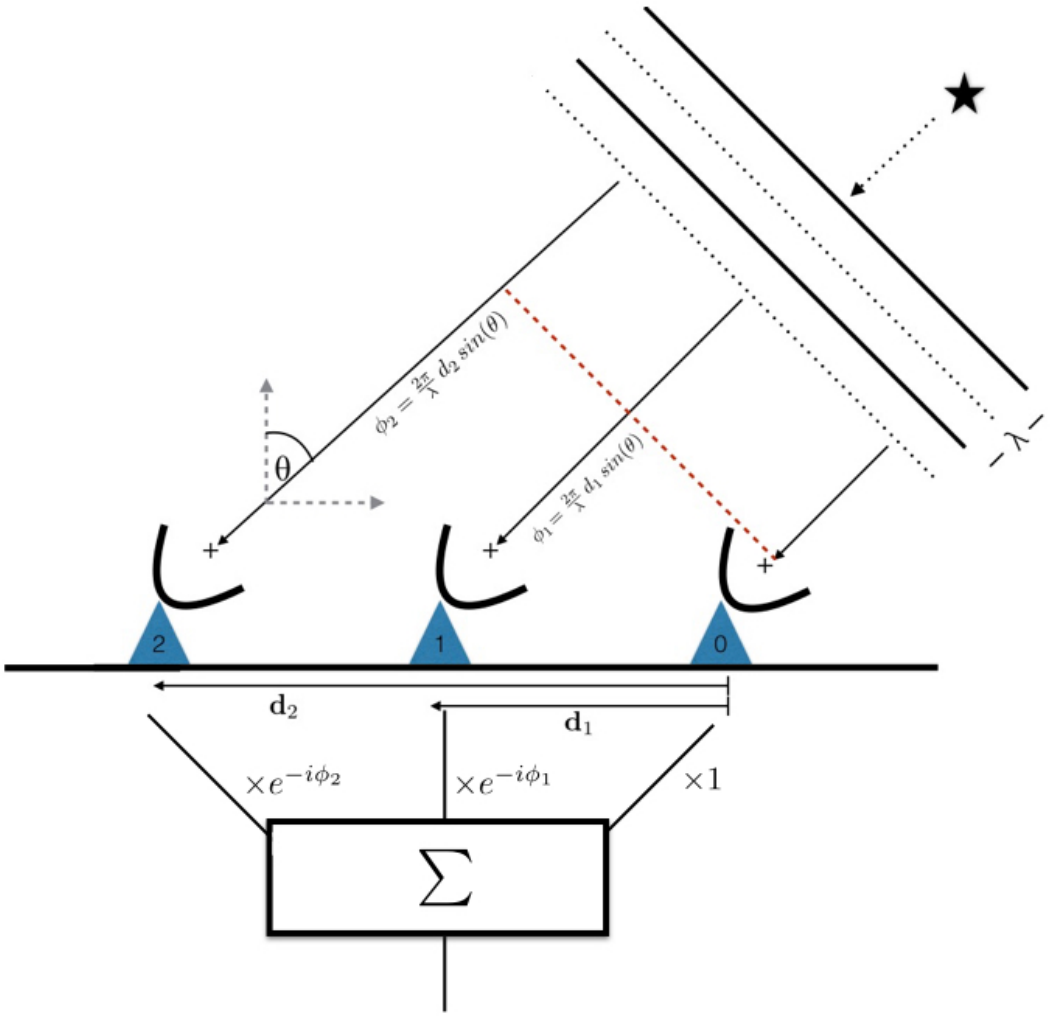

Figure 1.1: Diagrammatic example of a three-element beamformer. The wavefront from a far-field point-source arrives at each antenna at different times, but the delay is calculable given an array configuration and a direction to the object. Complex weights can be applied to each antenna's voltage time-stream to account for the geometric delay, allowing for the signals to be summed coherently.

$$\mathbf{d}_n \cdot \hat{\mathbf{k}} = \lambda \begin{pmatrix} u, & v, & w \end{pmatrix} \cdot \begin{pmatrix} -\cos\delta \sin HA \\ \cos(lat)\sin\delta - \sin(lat)\cos\delta\cos HA \\ \sin(lat)\sin\delta + \cos(lat)\cos\delta\cos HA \end{pmatrix}. \tag{1.10}$$

These phases are not only essential to beamforming but also for the fringestopping process, which is ubiquitous in interferometric analysis and is descibed in Sec. 1.4.1.

Variable	Coordinate
δ	Source declination
RA	Source right ascention
LST	Local sidereal time
HA	Source hour angle
alt	Source altitude
az	Source azimuth
lat	Telescope latitude
lon	Telescope longitude

1.4 Pathfinder beamformer

1.4.1 Instrumental phases

In a real experiment, if the voltages from each antenna, x_n, are summed without any adjustment as written in Eq 1.1, one should only expect noise and not a coherent beam. This is because we have assumed the wavefront's differential time-of-arrival across at array is the same time delay seen by the correlator. In fact each signal is further delayed by multiple steps in the signal chain. Digital phases in the electronics can be added by the LNAs and FLAs, and coaxial cables, whose lengths vary by up to a meter, can rotate the signal by multiple radians. Therefore in order to coherently sum across the array and beamform, the instrumental phases must be removed. If e_n is the true electric field on the sky as seen by each feed, then the thing we measure is the on-sky signal altered by an effective gain, g_n, and a noise term, n_n.

$$x_n = g_n e_n + n_n \tag{1.11}$$

We have lumped several terms into $g_n = |g_n| e^{i\phi_{g_n}}$, which is composed of a pointing-dependent beam term and any complex gain introduced after light hits the cylinder. Since we really only care about the phase, we can decompose $\arg(g_n)$ as,

$$\phi_{g_n} = \phi_{\text{beam}} + \phi_{\text{an}} + \phi_{\text{e}} + \phi_{\text{fpga}} \tag{1.12}$$

where ϕ_{beam} is the beam's phase for a given pointing, ϕ_{an} comes from the analogue chain (dual-pol feed, coax, etc.), ϕ_{e} is any phase introduced in the electronics, and ϕ_{fpga} are phases applied in the F-engine.

Since the instrumental phases are effectively random, the simplest way to remove them is to solve for them empirically, usually from a point-source on the sky. Using the visibility definition in Eq 1.16, one can evaluate that all-sky integral assuming the sky's

electric field is produced by a single point-source. This is tantamount to a delta function at a single direction on the sky.

$$V^{\rm ps}_{m,n} = \int d^2\hat{\mathbf{k}}\, g_m(\hat{\mathbf{k}})\, g^*_n(\hat{\mathbf{k}})\, e_m(\hat{\mathbf{k}}) e^*_n(\hat{\mathbf{k}})\, \delta(\hat{\mathbf{k}} - \hat{\mathbf{k}}_{\rm ps}) \tag{1.13}$$

$$= g_m(\hat{\mathbf{k}}_{\rm ps})\, g^*_n(\hat{\mathbf{k}}_{\rm ps})\, e_m(\hat{\mathbf{k}}_{\rm ps}) e^*_n(\hat{\mathbf{k}}_{\rm ps}) \tag{1.14}$$

In this equation $\hat{\mathbf{k}}_{\rm ps}$ is the only direction on the sky with a source — an approximation whose validity we will discuss below — and δ is a Kronecker delta function.

$$V^{\rm ps}_{m,n} = \tag{1.15}$$

$$V_{m,n} = \int d^2\hat{\mathbf{k}}\, g_m(\hat{\mathbf{k}})\, g^*_n(\hat{\mathbf{k}})\, e_m(\hat{\mathbf{k}}) e^*_n(\hat{\mathbf{k}}) \tag{1.16}$$

If we explicitly write the phase information of the sky's electric field, we can use

$$e_m(\hat{\mathbf{k}}) e^*_n(\hat{\mathbf{k}}) = T(\hat{\mathbf{k}}) e^{2\pi i\, \hat{\mathbf{k}}\cdot\mathbf{d}_{mn}}. \tag{1.17}$$

$$V_{m,n} = \int d^2\hat{\mathbf{k}}\, g_m(\hat{\mathbf{k}})\, g^*_n(\hat{\mathbf{k}})\, T(\hat{\mathbf{k}}) e^{2\pi i\, \hat{\mathbf{k}}\cdot\mathbf{d}_{mn}} \tag{1.18}$$

Therefore a single correlation can be written as an intensity multiplied by a phase factor that is determined by the source-position's projection onto that correlation's baseline. Since that phase factor is calculable via Eq. 1.10, it can be removed in a process called "fringestopping". The data can be inspected visually quite easily, since a transiting point-source will fringe as a function of time at a rate corresponding to the projected baseline length, but should not after fringestopping is applied. This is demonstrated with an inter-cylinder Cygnus A transit in Fig. 1.4.1.

The $N(N+1)/2$ visibilities we measure can be thought of as the upper triangle of an $N \times N$ complex Hermitian matrix, $\mathbf{V}$. This is simply the outer product of the signal vector, $\mathbf{x}$, with its Hermitian conjugate.

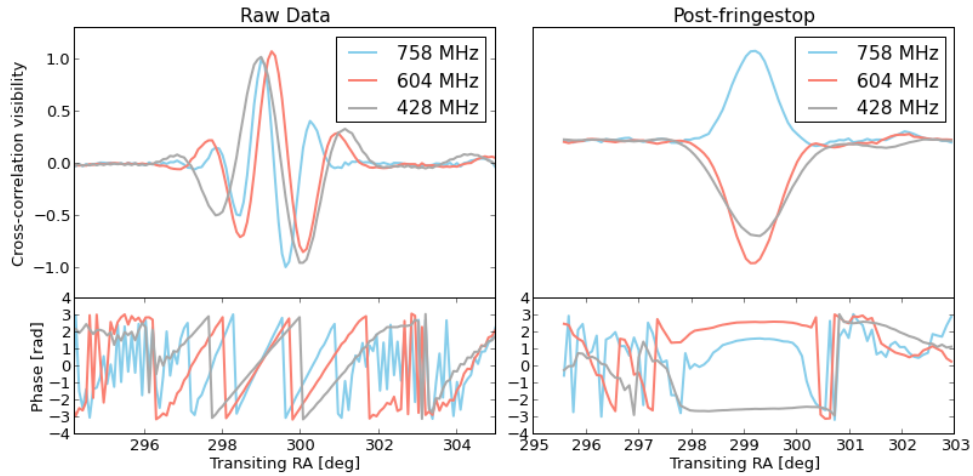

Figure 1.2: An example of the fringestopping process that is necessary for gain calibration off of a transiting point-source. Since the phase of a visibility will have a time- and frequency-dependent component, the measured correlation will fringe as the earth rotates in a chromatic way. This effect can be removed by multiplying each visibility by $e^{-i\phi_{\rm mn}({\rm t},\nu)}$, as determined by Eq. 1.10. The top left panel shows the raw correlation as a function of transiting RA between feeds 1 and 129, which are of the same polarization but on opposite cylinders, separated by 21 m. We plot three different frequencies. The panel below it shows the same complex visibility's phase. The slope, or fringe-rate, decreases at lower frequencies, as expected. The right panel show the same data after running it through the fringestopping pipeline. Though the resulting phases are near flat, implying that the baseline is no long fringeing, the visibilities are not purely real; this is because there are residual instrumental phases. These phases can be solved for using an eigendecomposition now that the array is phased up to a single point-source.

$$\mathbf{V} = \mathbf{x}\mathbf{x}^{\dagger} \approx \begin{pmatrix} |g_0|^2\, e_0^2 & \cdots & \\ & g_n g_m^* e_n e_m^* & \\ & \ddots & \\ & & |g_N|^2\, e_N^2 \end{pmatrix} \tag{1.19}$$

If the sky is composed of a single point-source then this matrix will be rank one, i.e. there is only one non-zero eigenvalue. One can see this by referring to Eq. 1.17 and noting that if the data has been fringestopped, then the sky temperature can be factored out of Eq. 1.19, which becomes

$$\mathbf{V} = T(\hat{\mathbf{k}})\,\mathbf{g}\mathbf{g}^{\dagger}. \tag{1.20}$$

Therefore by diagonalizing the correlation matrix $\mathbf{V}$ we get a complex eigenvector corresponding to the largest eigenvalue, that is proportional to the gain vector $\mathbf{g}$. The phase of this eigenvector will be an estimate for the instrumental phases, ϕ_{g_n}, up to some unknown global offset. The goodness of this calibration depends on the validity of our assumption that the correlation matrix is rank one. We can estimate the error on the calibration solution as the ratio of the second largest eigenvalue, λ_2, to the largest, λ_1. For typical frequencies we get values of $\frac{\lambda_2}{\lambda_1} \sim 3\%$.

These algorithms have been implemented in a pre-beamforming pipeline written in `Python`. Each day a point-source transit is fringestopped and a calibration solution is solved for. The source chosen depends on the solar time of its transit: Since the sun is extraordinarily bright in our band, the transit has to be at night for good calibration solutions. Historically, we have used Cygnus A in the spring and summer, Cassiopeia A in the summer and fall, and Tau A in the winter. Whatever we calibrate off of, the phases of that solution are written to pickle files that are readable by the Pathfinder's FPGAs. The FPGA then applies complex gains after channelization, which in theory should provide the beamforming kernel with voltages whose phases are purely geometric.

1.5 FRB VLBI search

1.6 Conclusion

Acknowledgements

We thank Ondrej and Nolan and Peterman.

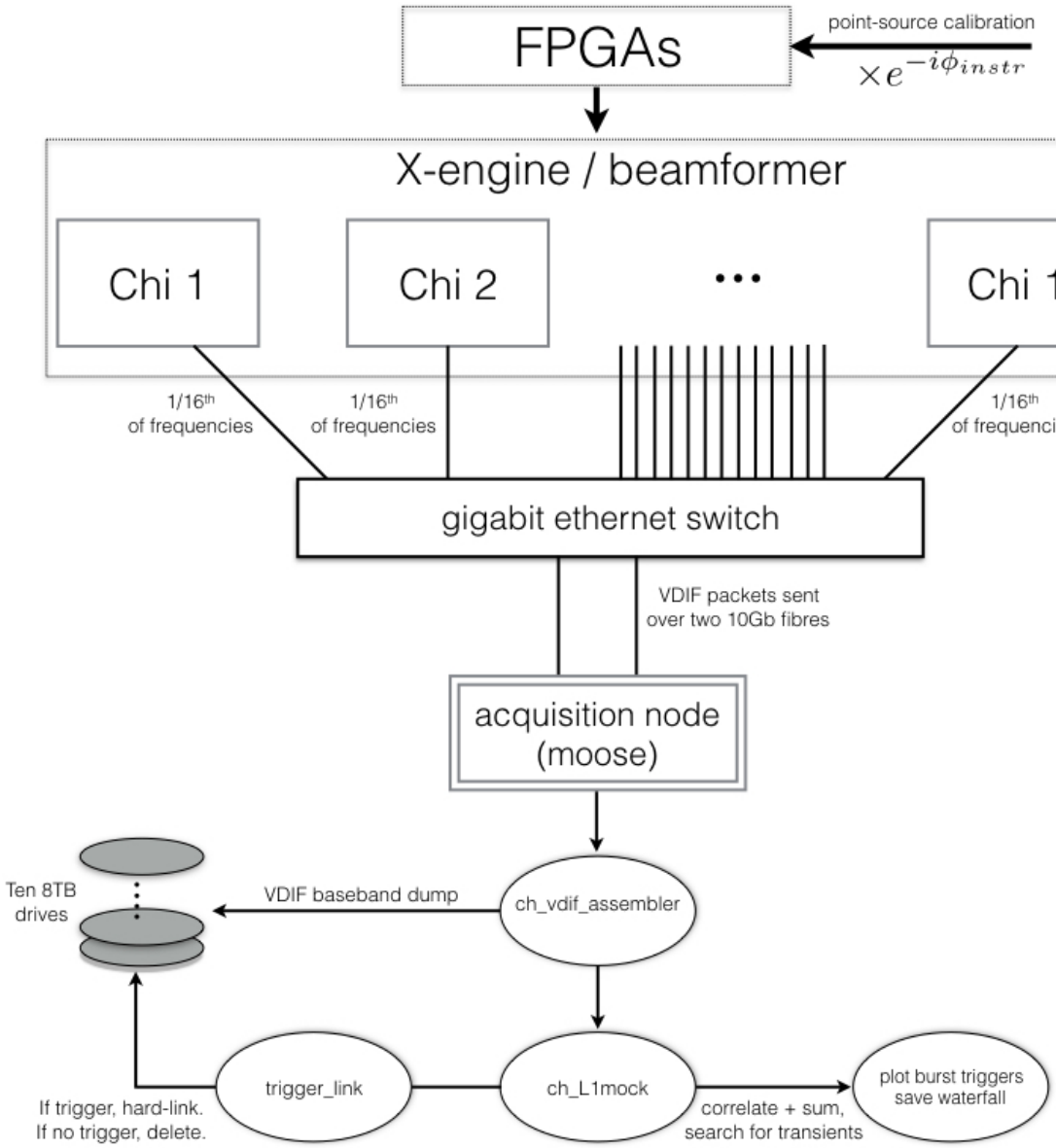

Figure 1.3: Block diagram of the beamforming backend on CHIME Pathfinder. A calibration solution is obtained from a bright point-source transit, the phases of which are fed into the FPGAs where they are applied as a digital gain. All antenna signals are then sent the X-engine, comprised of 16 GPU nodes. Each node applies geometric phases then sums the voltage stream across all antennas with the same polarization. The two resultant beams are then sent to our acquisition machine `moose` as `VDIF` packets, where a multi-threaded capture code, `ch_vdif_assembler`. At this point the baseband data are either written to disk as scrambled baseband `VDIF`, or they are reorganized in time and frequency. The ordered data are searched for FRBs after squaring and integrating to ∼millisecond cadence using a tree-dedispersion algorithm. If there is a trigger, then the corresponding baseband data is hard-linked. Old files that haven't been hard-linked are deleted periodically.